Acoustic study of dislocation rearrangement at later stages of fatigue: Noncontact prediction of remaining life

Hirotsugu Ogi,[a] Yoshikiyo Minami, and Masahiko Hirao
Graduate School of Engineering Science, Osaka University, Machikaneyama 1-3, Toyonaka, Osaka 560-8531, Japan

(Received 28 August 2001; accepted for publication 13 November 2001)

This study is devoted to clarifying the mechanism of the surface-shear-wave attenuation peak observed during rotating bending fatigue of carbon steels. We have developed electromagnetic acoustic resonance to make a contactless monitoring of the attenuation throughout the fatigue test. The attenuation peak occurs at a fixed fraction to lifetime, being independent of the bending stress (0.49–1.20 of the yield stresses) and the carbon content (0.22–0.45 mass %). Low-temperature heat treatment reduces the peak attenuation back to the previous value, which indicates a dominant contribution of dislocations. Microstructure observations with transmission electron microscopy, surface crack study with replicas and the acoustic measurements show that a large-scale change occurs in the dislocation structure (persistent slip bands to cells) at the attenuation peak and that it is triggered by the inward growth of cracks. This change is completed in a short time, a few percent of the total lifetime. The acoustic-resonance technique can be an important means for the exact prediction of the remaining life of fatigued steels. © *2002 American Institute of Physics.*
[DOI: 10.1063/1.1433178]

I. INTRODUCTION

Numerous studies on fatigue of metallic materials have been published to date. They include observations of microstructures in the incubation period (small cracks, slip bands, dislocations, etc), nondestructive evaluation of materials deterioration using several physical phenomena, and fracture mechanics as summarized in some excellent monographs.[1,2] These efforts contributed to make an essential view of fatigue and physics behind it clear. Adding to these extensive studies, we have recently suggested a dislocation-structure evolution, which finishes within a short period in the later stages of rotating bending fatigue of a 0.45 mass % C steel and aluminum alloy.[3] Ultrasonic attenuation showed one or two sharp peaks at the later stages, and aging the specimen at room temperature or exposing it to a low-temperature heat treatment considerably lowered the peak attenuation. This strongly indicates that dislocations play the principal role in the attenuation peak.

Such an instantaneous microstructure change has not been observed despite the long history of study. There are two main reasons for this. First, as a nature of fatigue, the fatigue life can be widely variable even for the same loading condition and material. The number of elapsed cycles never tells the current deterioration degree and the remaining life. (Fracture mechanics is only applicable to know the growth rate of large cracks, if they are well identified and the stress field around them is measurable.) Then, the repeatable study at a prescribed fractional life to fracture has never been realized. Second, there was no method of continuously measuring the evolution of interior microstructure change throughout the fatigue life. It should be nondestructive and have enough sensitivity to the dislocations below surfaces but no influence to the fatigue process. So far, electromagnetic acoustic resonance (EMAR) can only do this task as has been demonstrated. In our companion studies for copper[4] and 0.15 mass % carbon steel,[5] the EMAR method detected the processes of dislocation activity including the formation of cells at the early stages of zero-to-tension and pull–push fatigue.

In this study, we elucidate the mechanism of the instantaneous change of ultrasonic attenuation, which seems to be associated with dislocation activity and crack growth. We performed *in situ* monitoring of the surface-shear-wave attenuation during rotating bending fatigue of carbon steels. The attenuation peak appeared at the later stages and the microstructure change around the peak was studied by transmission electron microscopy (TEM). We observed the evidential event in the dislocation structure at the attenuation peak.

II. MATERIALS

We used commercial steel rods containing 0.22, 0.35, and 0.45 mass % carbon. They were heated at 880 °C for 1 h and cooled in air. Table I gives their chemical compositions and yield strengths. The specimen diameter was smoothly decreased with a large curvature to cause failure at the minimum diameter of 14 mm, where ultrasonic attenuation was measured. We electrically polished the specimen surface before the fatigue test.

III. MEASUREMENT

Many studies measured the ultrasonic characteristics (velocity, attenuation, nonlinearly, etc.) during fatigue tests,[6–9] but none of them observed such an important phenomenon occurring at the later stages. This is because they

[a]Author to whom correspondence should be addressed; electronic mail: ogi@me.es.osaka-u.ac.jp

TABLE I. Chemical compositions (mass %) and the yield strengths (MPa) of the carbon steels.

	C	Si	Mn	P	S	Cu	Cr	Ni	Yield strength
0.22 mass %C steel	0.22	0.19	0.41	0.18	0.15	0.02	0.06	0.01	333
0.35 mass %C steel	0.35	0.18	0.64	0.20	0.11	0.10	0.15	0.06	449
0.45 mass %C steel	0.45	0.18	0.64	0.21	0.18	0.13	0.11	0.06	471

all employed conventional contacting measurements and the large background obscured the sensitivity to the microstructures. This is an especially serious problem in the attenuation measurement because mechanical contacts allow the probing ultrasonic wave to propagate in the couplant and the transducer, not only in the specimen, and much acoustic energy is absorbed during propagation in them. It is then clear that contactless measurements with electromagnetic acoustic transducers (EMATs) are preferable, but the weak transfer efficiency prevented us from measuring the ultrasonic characteristics with enough accuracy. To overcome this dilemma, we used an EMAT in the resonance method so as to superimpose many signals coherently and compose large signal amplitudes. This is the EMAR method developed for the contactless monitoring of the phase velocity and attenuation.[10]

Our measurement setup is shown in Fig. 1, which is basically the same as the previous study.[3] The EMAT consists of the solenoid coil to apply the bias magnetic field in the specimen axial direction and the meander-line coil to induce the dynamic field in the circumferential direction. When sinusoidal current is applied to the meander-line coil, the total field oscillates about the axial direction at the same frequency as the driving current and produces shearing vibration through the magnetostrictive effect to excite the axial shear wave propagating along the circumference with axial polarization.[11] The meander-line coil also receives the axial shear wave through the reverse magnetostrictive effect. Excitation with long tone bursts causes interference among the axial shear waves and a frequency scan detects resonance peaks at unequal intervals, at which all the waves overlap coherently to produce large amplitudes.

The resonance frequencies are determined by the elastodynamic equation and the stress-free boundary condition to be a solution of[12]

$$nJ_n(kR) - kRJ_{n+1}(kR) = 0. \tag{1}$$

Here, J_n denotes the nth Bessel function of the first kind, R the specimen radius, and $k = \omega/c$ the wave number with the angular frequency ω and the shear-wave velocity c. The integer n corresponds to the number of meandering along the circumference. In this study, we used two meander-line coils; one has 0.9 mm periods and 20 mm axial length (coil A) and the other has 0.44 mm periods and 10 mm axial length (coil B). Numerical calculation for Eq. (1) derives a series of resonance frequencies and corresponding amplitude distributions along the radius. The fundamental resonance frequency f appears at 3.89 and 7.94 MHz with coils A and B, respectively. Figure 2 shows the surface-wave-energy distribution for the fundamental modes generated by the two coils. The penetration depths are estimated to be 0.5 and 0.2 mm, respectively. We adopted the fundamental modes because they show the maximum amplitudes at the surface and decay with steep gradients with the radius. This property is suitable for concentrating the measurement at the thin surface layer and detecting the microstructure evolution there due to rotating bending fatigue.

We determined the attenuation coefficients by fitting the exponential function to the free-decay amplitude at the resonance frequencies.[3,10] We rotated the specimens at 240 rpm (4 Hz). The bias field was fixed at 1.4×10^4 A/m. Four-point bending configuration produced the bending stresses at the measuring portion, which were varied between 140 and 490 MPa, corresponding to 0.42 and 1.2 to the yield strengths.

IV. MICROSTRUCTURE OBSERVATIONS

We obtained replicas of the specimen surface over the whole measurement area applying 70 MPa bending stress to open the cracks, and measured the number of cracks and their lengths. We determined the maximum crack length and calculated the crack density from the total crack lengths divided by the viewing area.

At the representative stages of the attenuation evolution, we stopped the fatigue test and observed the dislocation

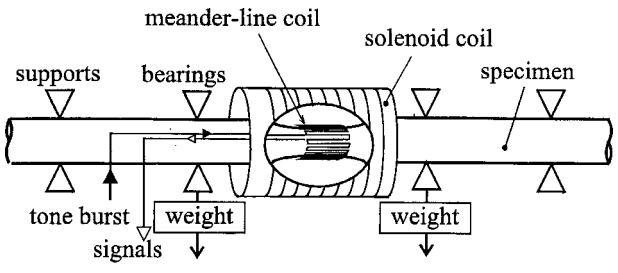

FIG. 1. Measurement setup of the rotating–bending–fatigue test.

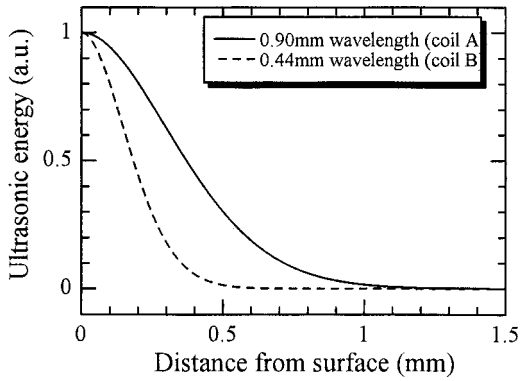

FIG. 2. Decay of the axial-shear-wave energy at the fundamental resonance modes.

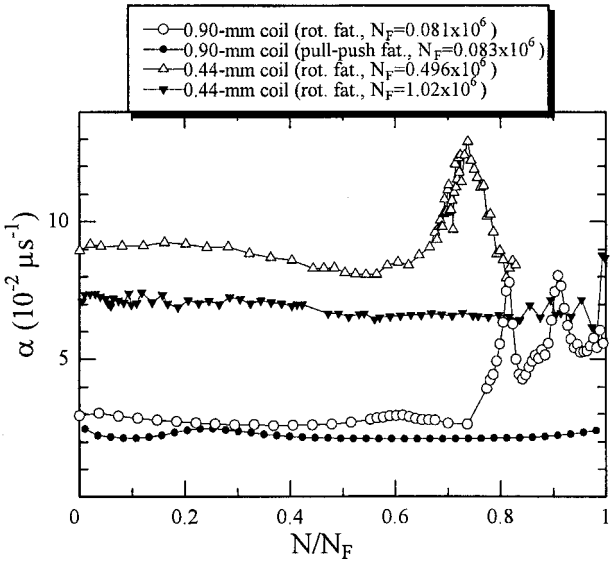

FIG. 3. Evolutions of the attenuation coefficient during rotating bending fatigue and pull–push fatigue for the 0.22 mass % C steel. The number of cycles N is normalized by the failure cycle number N_F.

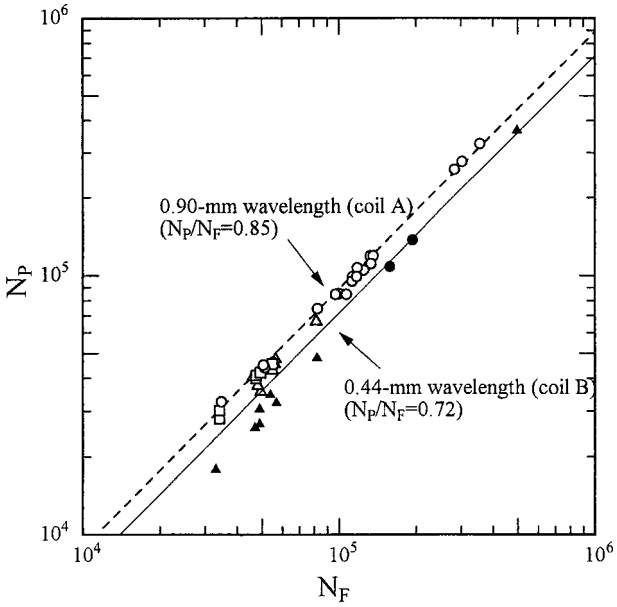

FIG. 4. Failure cycle number N_F vs the cycle number at the attenuation peak N_P. Open marks denote measurements by coil A and closed marks denote those by coil B. Circles, squares, and triangles denote the measurements for 0.22, 0.35, and 0.45 mass %C steels, respectively.

structure by TEM. (Nonstop attenuation monitoring is available.)[3] Thin samples were carefully cut from the fatigued specimens to about 0.4 mm thick involving the specimen surface using a low-speed electrical-discharge wire. Polishing on the emery paper made them about 100 μm thick. A jet electropolishing apparatus introduced a small hole at the center of the foil with electrolyte of 8% perchloric acid, 10% 2-butoxyethanol, 70% ethanol, and water. TEM images were then obtained around the hole.

V. RESULTS

Figure 3 shows typical changes of the attenuation coefficient α. It remained unchanged for a long time and then showed remarkable peak(s). We interrupted the fatigue test at the attenuation peak and exposed the specimen to the low-temperature heat treatment at 300 °C for 1 h; the attenuation returned to that before the peak.

Figure 4 plots the cycle number to failure N_F versus the cycle number at the attenuation peak N_P. The attenuation peak appeared earlier with coil B ($N_P/N_F=0.72$) than with coil A ($N_P/N_F=0.85$). The ratio N_P/N_F appears to be independent of carbon content and the bending stress, indicating a potential capability of evaluating the remaining life. However, α remained unchanged throughout the life, when the bending stress was so small that N_F was beyond 1 000 000 (solid triangles in Fig. 3).

Removal of the deteriorated surface layer delayed the peak. We interrupted the fatigue test prior to the attenuation peak, electrically polished the specimen surface to remove the damaged layer about 0.3 mm thick, and then restarted fatiguing. As shown in Fig. 5, which is measured by coil A, the attenuation peak was delayed to appear ($N_P/N_F \sim 0.93$), but the ratio N_P/N_F was unchanged (~ 0.87) if the cycle number was counted from the restarting point.

Figure 6 shows the crack evolution. Surface cracks were observable with an optical microscope as early as at about 25% of lifetime. The crack density monotonically increased since then, while the maximum length remained small until about 80% and rapidly increased to failure. We observe that cracks nucleate at the early stages and then the crack density increases, keeping their lengths nearly unchanged. After 80%, the small cracks coalesce with each other, finally leading to their inward growth.

Figures 7(a)–7(c) show the typical dislocation structures at 0.15 mm deep from the specimen surface before, at, and after the attenuation peak. Corresponding attenuation evolutions monitored with coil B are also shown. Because such a TEM micrograph provides very local information, we obtained many TEM images from the fatigued specimens with various bending stresses and identified the representative dislocation structure at each stage.

We found few dislocations in the annealed specimen before fatigue. Before the attenuation peak [Fig. 7(a)], many

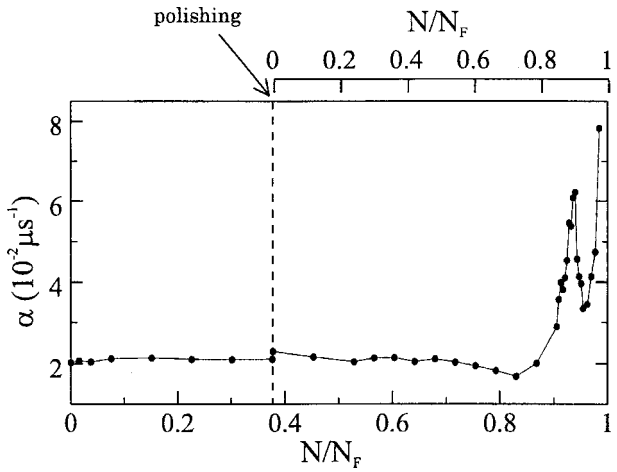

FIG. 5. Attenuation evolution after removing the damaged surface layer (0.45 mass % C steel).

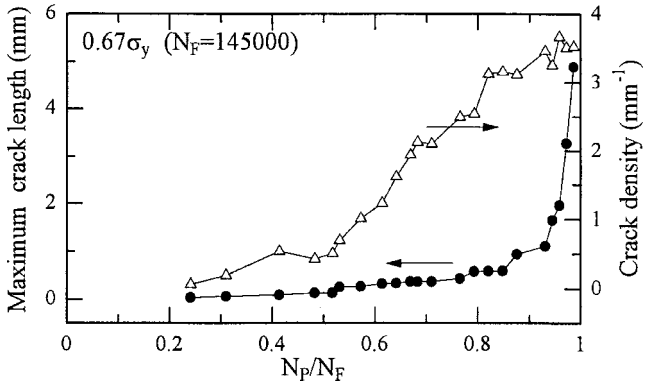

FIG. 6. Changes of the maximum crack length and crack density with progress of rotating–bending–fatigue (0.22 mass % C steel).

dislocation walls about 0.2 μm thick occurred, which were aligned parallel with nearly constant spacing about 1 μm. There were few dislocations between the walls. At the attenuation peak [Fig. 7(b)], many single-line dislocations were bridging the walls. After the attenuation peak, the dislocation-wall structures were divided into smaller cells with few dislocations inside [Fig. 7(c)]. Similar dislocation-structure evolution was observed around the attenuation peak measured with coil A at 0.3 mm thickness from surface.

VI. DISCUSSION

First of all, the attenuation recovery after the heat treatment excludes the possibility of the cracks' direct contribution to the attenuation evolution. Figure 5 shows that the attenuation change was caused by the microstructure behavior within the thin surface layer. We then attribute the attenuation evolution to the dislocation-structure change in the surface region. However, we should note that the attenuation peak tells the remaining life (Fig. 4), which is controlled by cracking. Therefore, seeking an interrelation among attenuation, dislocations, and cracks, we shall discuss our results in terms of:

(i) dislocation damping theory,
(ii) dislocation mobility,
(iii) crack-tip zones and dislocation evolution, and
(iv) volume fraction of the crack-tip zone to the surface-wave propagating region.

Among all crystal defects contributing to attenuation, only dislocations cause such a nonmonotonous evolution of attenuation. Granato–Lücke theory[13] relates attenuation α to the density Λ and the length between pinning points L of the effective dislocations that can vibrate responding to the acoustic wave. Because of the phonon viscosity, the vibration is anelastic, causing the loss. In frequencies much lower than the dislocation-segment resonance frequency ($\sim$0.1 GHz), the relationship reduces to $\alpha \sim \Lambda L^4 f^2$, indicating that α increases with the effective dislocations. Thus, the theory can explain the attenuation evolution, provided that the dislocations bridging the walls [Fig. 7(b)] are effective and that the densely gathering dislocations in the walls are ineffective (immobile). Also, this theory explains larger background attenuation with coil B than with coil A in Fig. 3; the resonance frequency of coil A is nearly half of coil B's.

In fatigued fcc crystals, very similar dislocation structures to Figs. 7(a) and 7(b) have been reported.[14,15] Those are known as persistent slip bands (PSBs), consisting of the dense array of dislocations (walls) and the sparse zone between the walls. The dislocation walls are mainly made up with edge-dislocation dipoles (pairs of opposite-sing dislocations), which strongly attract each other and will be immobile with the acoustic wave. Such a PSB structure was also observed for polycrystalline low-carbon steels by Phol *et al.*,[15] and the dislocation structures observed before and at the attenuation peak appear to be the PSBs. We consider that the dislocations bridging the walls [Fig. 7(b)] are mobile and they are the very cause of raising attenuation. Indeed, they appear and glide when local plastic deformation occurs in the PSBs.[1] These dislocations will gather by further cyclic loading to divide the between-wall areas, resulting in cells with few dislocations inside. The transition from the PSBs to cells was also observed in carbon steels.[15] Our previous study[4] revealed that the dislocation cells absorb little acoustic energy. Thus, the attenuation peak can be explained by the microstructure rearrangement from the PSBs to the cells, during which many mobile dislocations are temporarily created to absorb the acoustic energy.

Phol *et al.*[15] indicated that the transition required sufficiently large stress amplitude. Our view is that this can be made possible by crack growth even for lower cyclic stress amplitude. There is a highly stress-concentrated zone ahead of a crack tip, which causes local plastic deformation and then the dislocation rearrangement. Indeed, as shown in Fig. 8, many small dislocation cells form around a crack tip and the microstructure is quite different from those far away from the tip.

Finally, we present a mechanism of the attenuation peak appearing at the fixed fractions to N_F (Fig. 4), which is schematically shown in Fig. 9. Dislocations will multiply from the beginning of fatigue throughout the lifetime, but most of them pile up to obstacles and tangle each other to shorten their lengths. The dislocation-density increase and the dislocation-length decrease balance each other and keep the attenuation unchanged for a long time. Meanwhile, the small cracks nucleate and the density increases while the average length changes little (see Fig. 6), indicating that the cyclic loading is spent by crack nucleation, not crack growth, due to the steep bending-stress gradient. The crack length was less than about 0.1 mm until the attenuation peak. Because the crack shape is a shallow semiellipsoidal one, the average crack is much shallower than the surface-wave penetration and the resultant tip zones are small. (The stress intensity factor at a crack edge increases with the crack depth.) Also, because of a lower number of cracks, the volume fraction of the total crack-tip zone to the whole shear-wave propagation region should be fairly small before the attenuation peak. The surface shear wave is then insensitive to the microstructure change at such a local region because an ultrasonic wave provides the averaged microstructure information over the propagation region. At the later stages, however, the dense surface cracks coalesce to grow not only along the circum-

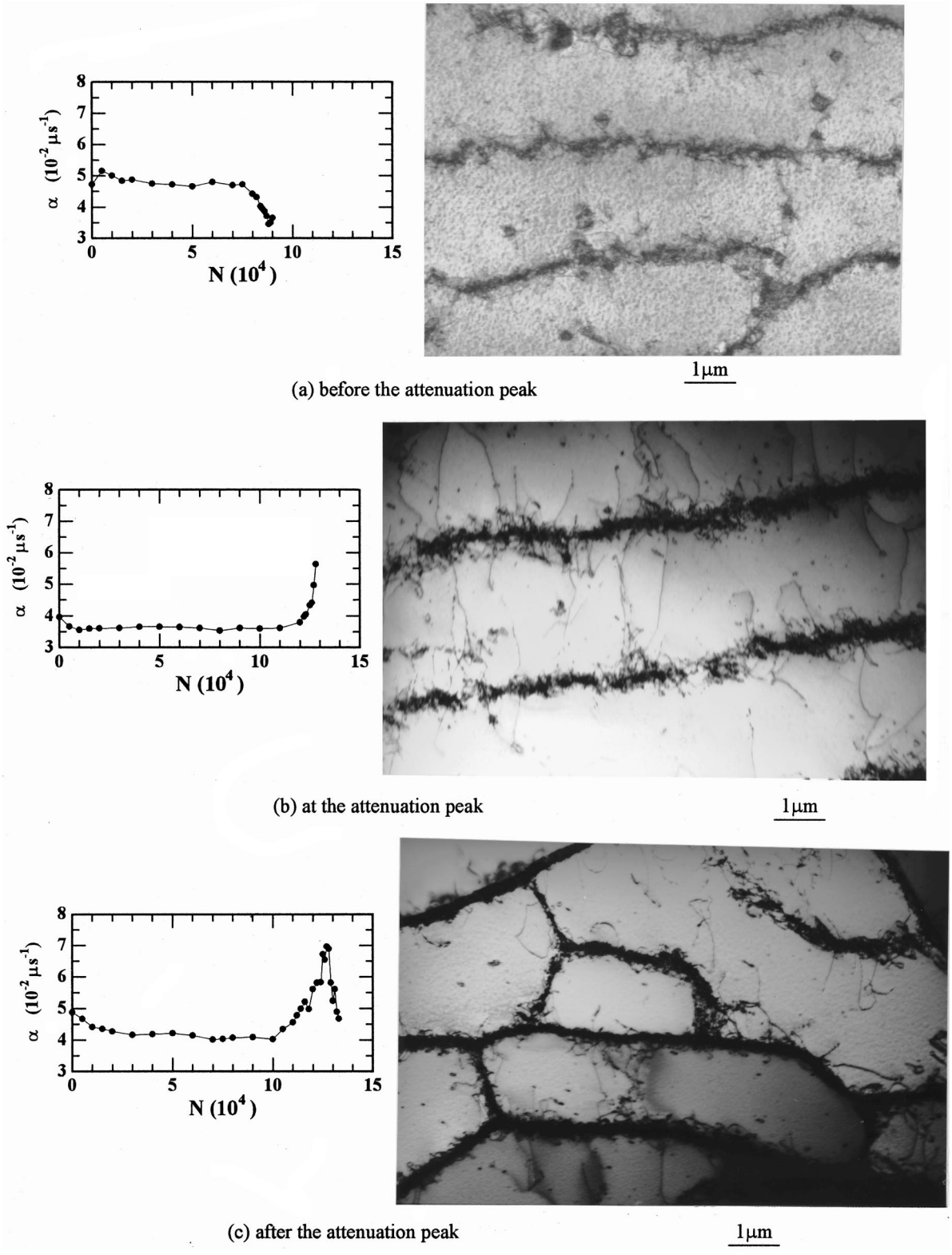

FIG. 7. Attenuation evolutions until the interruption and corresponding TEM micrographs: (a) before, (b) at, and (c) after the attenuation peak (0.45 mass % C steel).

ference but also inward, extending the tip zones toward the inside [Fig. 9(b)]. Then, the crack-tip-zone volume fraction to the proving-wave propagation region will be sufficiently large to give rise to a temporal increase in attenuation, responding to the microstructure evolution from the PSBs to the cells. With further cycling, the cracks extend further inside and the tip zones leave the surface-wave sensitive region [Fig. 9(c)]. Therefore, the shallower the surface-wave penetration, the earlier the attenuation peak is detected. The attenuation peak occasionally appeared twice as seen in Fig. 3.

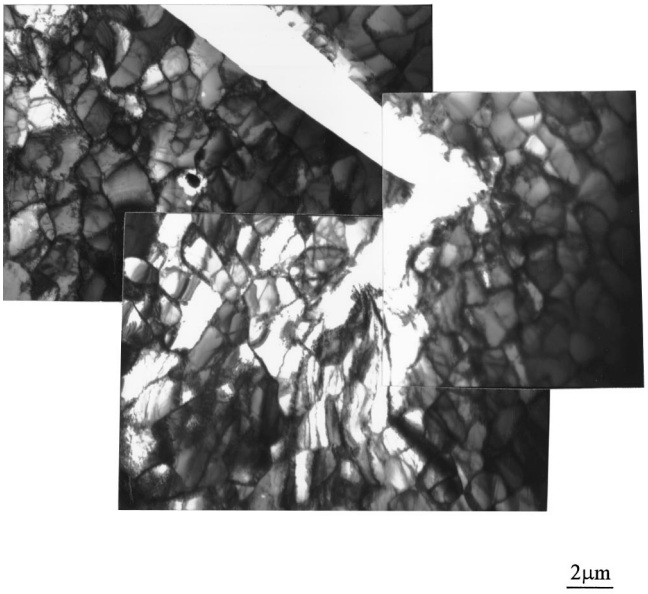

FIG. 8. Dislocation structure around the crack tip (0.45 mass % C steel).

This may reflect the dislocation rearrangement occurring at different positions within the proving region at different times.

After all, the key to observing the attenuation peak is the number of surface cracks. In Fig. 3, we add the attenuation evolution from the pull–push fatigue, where coil A was used. Despite the same material and the similar cycle number to failure, no attenuation peak appeared. A distinct difference was found in the crack-growth behavior. In the pull–push fatigue, very few surface cracks were visible and one of them grew inside to cause failure. Thus, the crack-tip zone occupies very little volume in the surface-wave propagation region, and the surface wave fails to detect such a highly localized microstructure change. This was also the case in very high-cycle rotation bending fatigue tests where the failure cycle number was beyond 1 000 000 cycles. Fewer cracks were observed again and only one of them grew toward failure. To detect the attenuation peak in these situations, we may need to decrease the axial length of the meander line to narrow the surface-wave propagation region.

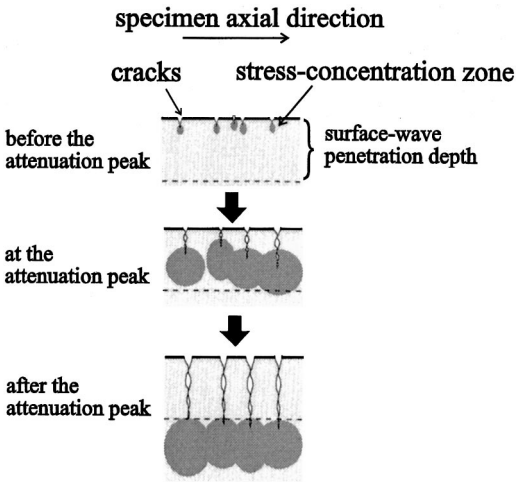

FIG. 9. Schematic explanation of the interaction between the dislocations and crack growth to cause the attenuation peak.

VII. CONCLUSION

The most important conclusion we reach from this study is that the dislocation-structure change from the PSBs to the cells does occur in a very short time at later stages, and the attenuation peak responds to this event. Because this change completes within a few percent of the total life, it is quite difficult to detect by other measurement methods and also by consulting the number of elapsed cycles.

Other principal conclusions are:

(1) The attenuation peak appeared at 85% and 72% of the total life with the measurements by 0.90 and 0.44 mm wavelength coils, respectively. This phenomenon always occurs, being independent of the carbon content and the bending stresses, so far as N_F is less than 10^6, and it is capable of predicting the remaining life.
(2) No attenuation peak appeared during the pull–push fatigue or the high-cycle rotating bending fatigue ($N_F > 10^6$) because of very few cracks.
(3) Dislocation damping theory is applicable to interpret the attenuation evolution. At the attenuation peak, many isolated dislocations bridging the dislocations walls appear. They are considered to be the direct cause of absorbing the acoustic energy.
(4) Such a microstructure evolution was triggered by the inward crack growth.

ACKNOWLEDGMENTS

Professor H. Mori and Dr. T. Sakata (Research Center for Ultra-High Voltage Electron Microscopy, Osaka University) helped the authors in obtaining the TEM micrographs in their facility. They also thank Dr. T. Ichitsubo (Graduate School of Engineering Science, Osaka University) for a valuable discussion on the results.

[1] S. Suresh, *Fatigue of Materials*, 2nd ed. (Cambridge University Press, Cambridge, 1998).
[2] M. Klesnil and P. Lukáš, *Fatigue of Metallic Materials* (Elsevier, New York, 1980).
[3] H. Ogi, T. Hamaguchi, and M. Hirao, Metall. Mater. Trans. A **31A**, 1121 (2000).
[4] M. Hirao, H. Ogi, N. Suzuki, and T. Ohtani, Acta Mater. **48**, 517 (2000).
[5] T. Ohtani, H. Ogi, and M. Hirao, J. Alloys Compd. **310**, 440 (2000).
[6] W. J. Bratina, in *Physical Acoustics IIIA*, edited by W. P. Mason (Academic, New York, 1966), pp. 268–291.
[7] R. Truell and A. Hikata, *Fatigue and Ultrasonic Attenuation* (ASTM, Philadelphia, PA, 1957), pp. 63–70.
[8] G. Fei and Z. Zhu, Phys. Status Solidi A **140**, 119 (1993).
[9] Z. Zhu and G. Fei, J. Alloys Compd. **211–212**, 93 (1994).
[10] M. Hirao and H. Ogi, Ultrasonics **35**, 413 (1997).
[11] H. Ogi, M. Hirao, and K. Minoura, *Review of Progress in QNDE*, edited by D. O. Thompson and D. E. Chimenti (Plenum, New York, 1996), Vol. 13, pp. 1939–1944.
[12] W. Johnson, B. A. Auld, and G. A. Alers, *Review of Progress in QNDE*, edited by D. O. Thompson and D. E. Chimenti (Plenum, New York, 1994), Vol. 13, pp. 1603–1609.
[13] A. Granato and K. Lücke, J. Appl. Phys. **27**, 583 (1956).
[14] H. Mughrabi, F. Ackermann, and K. Herz, in *Fatigue Mechanism*, Special Technical Publication 675 (ASTM, Philadelphia, 1979), pp. 69–105.
[15] K. Pohl, P. Mayr, and E. Macherauch, Scr. Metall. **14**, 1167 (1980).